Single-channel characterization of the chitooligosaccharide transporter chitoporin (*Sm*ChiP) from the opportunistic pathogen *Serratia marcescens*

Received for publication, May 1, 2022, and in revised form, September 8, 2022 Published, Papers in Press, September 14, 2022,
https://doi.org/10.1016/j.jbc.2022.102487

H. Sasimali M. Soysa[1], Sawitree Kumsaoad[2], Rawiporn Amornloetwattana[2], Takeshi Watanabe[3], and Wipa Suginta[2,*]

From the [1]School of Chemistry, Institute of Science, Suranaree University of Technology, Nakhon Ratchasima, Thailand; [2]School of Biomolecular Science and Engineering (BSE), Vidyasirimedhi Institute of Science and Technology (VISTEC), Rayong, Thailand; [3]Faculty of Agro-Food Science, Department of Agro-Food Science, Niigata Agro-Food University, Niigata, Japan

Edited by Robert Haltiwanger

***Serratia marcescens* is an opportunistic pathogen that can utilize chitin as a carbon source, through its ability to produce chitin-degrading enzymes to digest chitin and membrane transporters to transport the degradation products (chitooligosaccharides) into the cells. Further characterization of these proteins is important to understand details of chitin metabolism. Here, we investigate the properties and function of the *S. marcescens* chitoporin, namely *Sm*ChiP, a chitooligosaccharide transporter. We show that *Sm*ChiP is a monomeric porin that forms a stable channel in artificial phospholipid membranes, with an average single-channel conductance of 0.5 ± 0.02 nS in 1 M KCl electrolyte. Additionally, we demonstrated that *Sm*ChiP allowed the passage of small molecules with a size exclusion limit of <300 Da and exhibited substrate specificity toward chitooligosaccharides, both in membrane and detergent-solubilized forms. We found that *Sm*ChiP interacted strongly with chitopentaose (K_d = 23 ± 2.0 μM) and chitohexaose (K_d = 17 ± 0.6 μM) but did not recognize nonchitose oligosaccharides (maltohexaose and cellohexaose). Given that *S. marcescens* can use chitin as a primary energy source, *Sm*ChiP may serve as a target for further development of nutrient-based antimicrobial therapies directed against multidrug antibiotic-resistant *S. marcescens* infections.**

Serratia marcescens is a facultative Gram-negative, soil-borne bacterium (1) that frequently causes outbreaks of community- or hospital-acquired infections in adults and children (2, 3). *S. marcescens* may cause respiratory infections (4, 5), meningitis (6, 7), and urinary tract infections (8). The microorganism is highly resistant to most antimicrobial agents (9–11). Numerous strains of *S. marcescens* possess quorum-sensing regulated virulence R factors, which are endogenous plasmids that carry antibiotic-resistance genes (12). Most strains also carry highly effective ABC-type efflux pumps (13). In addition, the cell envelope of *S. marcescens* has a complex lipopolysaccharide layer, which increases the bacterial membrane barrier. *S. marcescens* also forms biofilms (14–17). Treatment of *S. marcescens* infections can be difficult, owing to its intrinsic resistance to most antibiotics, including amoxicillin, ampicillin, the first generation of cephalosporins and carbapenems, and some fluoroquinolones (10, 18, 19). In severe cases, patients require intensive medical treatments using fourth-generation cephalosporins or piperacillin/tazoabactam (20).

S. marcescens can utilize various types of organic material as its carbon source and can produce chitin-active enzymes to hydrolyze chitinous materials and use them as an energy source (21). Chitin breakdown is initiated by a chitin-active lytic polysaccharide monooxygenase that breaks the chitin polysaccharide chain into chitin fragments by oxidative cleavage (22, 23). The oxidized chitin fragments are hydrolyzed further by chitinases (21, 22, 24–28) to short-chain chitooligosaccharides, which are transported into the periplasm of the bacterial cell through outer membrane (OM) porins. Previous studies reported the existence of several porins in the OM of *S. marcescens*, including Omp1, Omp2, Omp3, OmpF, and OmpC. These general diffusion pores take up small, hydrophilic molecules by passive diffusion (29, 30). On the other hand, a disaccharide (chitobiose) and higher molecular weight chitooligosaccharides, which cannot pass through the general diffusion pore, require a chitooligosaccharide-specific porin (ChiP) for their entry into the periplasm (24). Watanabe *et al.* (25) previously identified the *chiP* gene encoding ChiP (later named *Sm*ChiP) as part of the *chi*PQ-*ctb* gene cluster in the genome of *S. marcescens* 2170. The expression of *chiP* mRNA is controlled by the nontranslated *chiX* small RNA that binds to the gene's 5′-untranslated region, which contains a 17-nucleotide Shine-Dalgarno sequence preceding the *chi*PQ-*ctb* gene cluster. The same study also demonstrated that the *Δ*ChiP mutant had a drastically reduced growth comparing to the growth of the wildtype, confirming that ChiP played an important role in cell survival. We previously identified and characterized a chitooligosaccharide-specific porin, namely

* For correspondence: Wipa Suginta, wipa.s@vistec.ac.th.
Present address for H. Sasimali M. Soysa: Department of Physical Sciences and Technology, Faculty of Applied Sciences, Sabaragamuwa University of Sri Lanka, Belihuloya 70140 Sri Lanka.

*Sm*ChiP, from *S. marcescens* (31). In this report, we employed time-resolved single channel electrophysiology to examine the ion-conducting properties and substrate specificity of *Sm*ChiP. We also carried out *in vivo* cell studies to demonstrate that *S. marcescens* can employ chitooligosaccharides as its primary carbon source.

Results

Sequence analysis and AlphaFold2 structural prediction

We previously reported that some characterized chitoporins (ChiPs) exist as trimers and others as monomers, depending on the organism. For example, *Vf*ChiP identified from *Vibrio furnisii* (32), *Vh*ChiP from *Vibrio campbellii* (formerly classified as *Vibrio harveyi*) type strain ATCC BAA 1116 (33), and *Vc*ChiP from *Vibrio cholera* type strain O1 (34) are each composed of three identical subunits, while *Ec*ChiP from *Escherichia coli* is a monomeric porin (35, 36).

Figure 1 shows structure-based sequence alignment of monomeric ChiPs, including *Sm*ChiP and *Ec*ChiP, in comparison with trimeric ChiPs, including *Vh*ChiP and *Vc*ChiP. From the sequence alignment, *Sm*ChiP has high (77%) sequence identity with *Ec*ChiP, but low (17%) sequence identity with the trimeric ChiPs. The secondary structure elements of *Sm*ChiP are similar to those of *Ec*ChiP but different from those of the trimeric ChiPs. Overall, monomeric ChiPs have a single-barrel structure composed of 18 β-strands connected by eight extracellular loops, while *Vh*ChiP and other trimeric ChiPs contain 16 β-strands connected by eight extracellular loops. Loop L3 of trimeric ChiPs, which is typically identified as the pore-confining loop, is exceptionally long when compared with that of the monomeric ChiPs, while loops L2 and L6 of monomeric ChiPs are longer than those in the trimers. The *N*-terminal segment that is characteristic of trimeric ChiPs is longer than that of the monomeric ChiPs. Notably, the *N*-terminal segment of *Vh*ChiP contains a short helix that serves as the plug that regulates the open and closed states of the *Vh*ChiP pores (37). This *N*-plug is unique to *Vh*ChiP and is not present in other ChiPs (Fig. 1).

Figure 2 shows the AlphaFold2-predicted structure of *Sm*ChiP, compared with the crystal structure of the native *Vh*ChiP (PDB id: 5MDQ) (38). Figure 2*A* shows the side view (left panel) and top view (right panel) of *Vh*ChiP, consisting of three identical trimers, each of which contains the characteristic *N*-terminal plug, 19 amino acids long, with a short helix. In the closed channel, the *N*-plug of each monomer was found to plug the bottom half of the neighboring pore, causing the channel to close. The most prominent loop L3 (labeled green) contained three short helices, which folded inside the central part of the protein pore. This loop was the most important loop in *Vh*ChiP, in that it contained several amino acid residues that bound to the sugar substrate (chitohexaose) (38). Figure 2*B* (left panel) shows the side view of the monomeric *Sm*ChiP barrel, lacking the *N*-plug. Although loop L3 of *Sm*ChiP also protruded into the protein pore, it was not helical, leaving more space inside the channel interior (Fig. 2*B*, right panel). Superimposition of *Sm*ChiP onto one monomer of *Vh*ChiP yielded an R.M.S.D. of 3.75 Å for 940 atoms, reflecting large differences in the amino acid arrangement inside the two

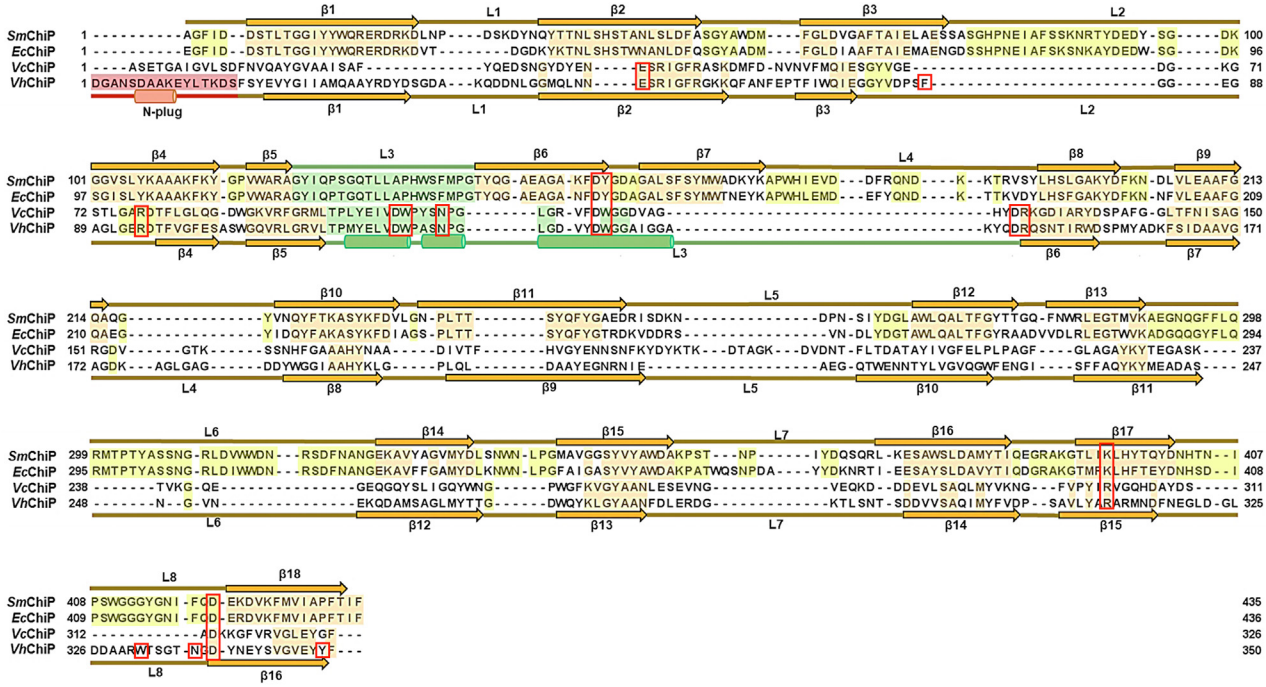

Figure 1. Structure-based sequence alignment of four characterized chitoporins: *Sm*ChiP (protein id: A0A0PBS3), *Ec*ChiP (protein id: P75733), *Vc*ChiP (protein id: Q9KTD0), and *Vh*ChiP (protein id: L0RYU0). The amino acid sequences of these proteins were aligned by MAFFT alignment and displayed in Jalview *v.* 2.11.2.1. The 2D structural elements of monomeric *Sm*ChiP, displayed at the *top*, were constructed from AlphaFold2 (https://alphafold.ebi.ac.uk/), while the 2D structural elements of trimeric *Vh*ChiP, displayed at the *bottom*, were constructed from the crystal structure of the native form (PDB id: 5MDQ). Helices are represented by *cylinders*, β-strands by *thick arrows*, and loops by *lines*. *Sm*ChiP, *Serratia marcescens* chitoporin.

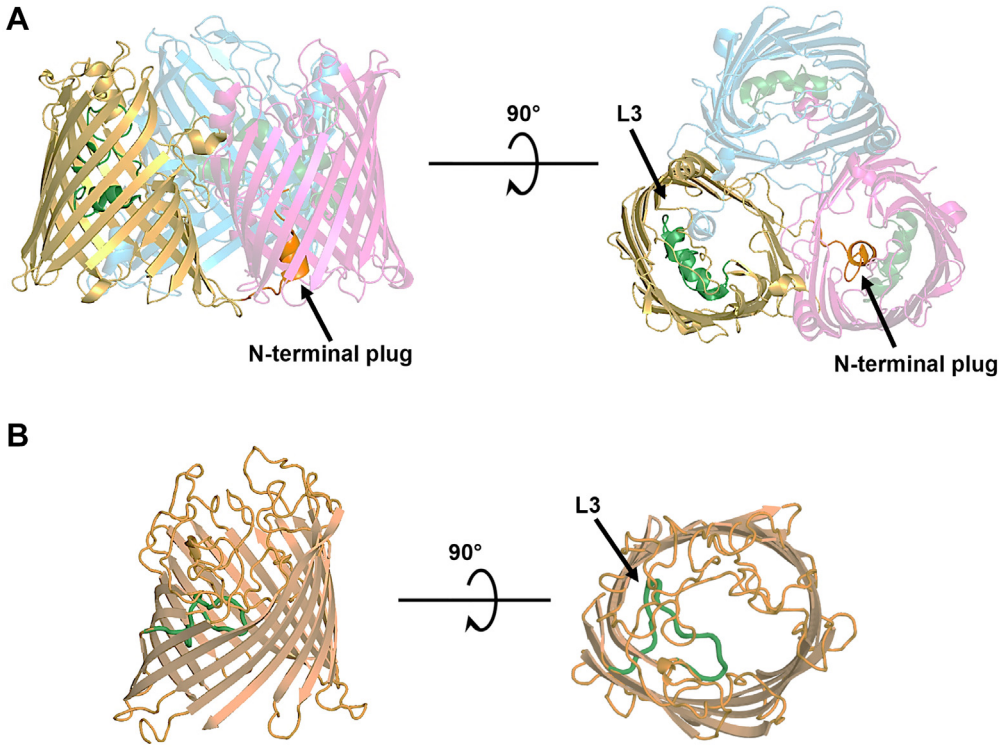

Figure 2. The overall structures of *Vh*ChiP and *Sm*ChiP. *A*, *Vh*ChiP. *B*, *Sm*ChiP. The structure of *Sm*ChiP was predicted by AlphaFold2 (https://alphafold.ebi.ac.uk/) as described in text, while the structure of *Vh*ChiP was retrieved from the PDB database (PDB id: 5MDQ). *Sm*ChiP, *Serratia marcescens* chitoporin.

channels. We found a few residues that are conserved but were unable to identify the amino acid residues inside the *Sm*ChiP pore that could form the substrate binding sites, due to the high diversity in amino acid sequences between *Sm*ChiP and *Vh*ChiP.

Determination of the molecular weight of native SmChiP

The native state of the OM-expressed *Sm*ChiP was determined by size exclusion chromatography. Figure 3 shows the elution profiles of the protein standards together with *Sm*ChiP, using a HiPrep 26/60 prepacked Sephacryl S-300 column. *Sm*ChiP was eluted at a position between ovalbumin (43 kDa) and bovine serum albumin (66 kDa) (Fig. 3*A*). The eluted fractions obtained from the A_{280} peak were pooled and analyzed by SDS-PAGE. Figure 3*A* (inset) shows a Coomassie-stained protein band, which migrated at about 45 kDa, consistent with the apparent molecular mass of 50 kDa of *Sm*ChiP determined from the distribution coefficient (K_{av}) (Fig. 3*B*) and confirming that *Sm*ChiP is a monomer.

Single-channel electrophysiology

Single-channel measurements were carried out with lipid bilayer measurements (BLM) *Sm*ChiP reconstituted in 1,2-diphytanoyl-sn-glycero-3-phosphocholine membranes, and ion flow through the membrane-embedded *Sm*ChiP was recorded at different applied potentials. Figure 4, *A* and *B* show representative ion current traces acquired over 2000 ms at +100 mV and −100 mV, respectively. The channel was also found to be constantly open within a wide range of applied transmembrane potentials from ±25 mV to ±150 mV (data not shown).

Ion traces acquired from a single *Sm*ChiP channel exhibited single-step openings with no subconductance or gating, at both negative and positive potentials. A current magnitude of approximately 50 pA was consistently observed under the applied potentials of ±100 mV in 1 M KCl electrolyte, giving the average single channel conductance of 0.5 nS (G = 0.5 nS). This conductance value of *Sm*ChiP is about one-third of that of trimeric *Vh*ChiP (G = 1.8 ± 0.3 nS) (39), consistent with the monomeric structure of the *Sm*ChiP channel. Multichannel reconstitution experiments (Fig. 4*C*) further confirmed the mean channel conductance of 0.54 ± 0.2 nS from 60 independent channel insertions, obtained from Gaussian distribution fitting of the histogram (Fig. 4*D*). The channel conductance obtained from the I-V plot (Fig. 4*E*, for nine independent insertions) was 0.54 ± 0.01 nS, which was essentially identical with the value obtained from the multichannel insertions shown in Figure 4*C*.

Sugar selectivity of SmChiP *at single-channel level*

In this series of experiments, we examined the substrate specificity of *Sm*ChiP by exposing the channel to different chitooligosaccharides and examining their transient blocking behavior. In the absence of sugar, *Sm*ChiP was fully open, allowing a steady ionic current over the entire recording time of 2 min at both applied negative and positive potentials. Figure 5*A* shows a representative ion trace of an empty channel, which had ionic conductance of −50 pA at −100 mV

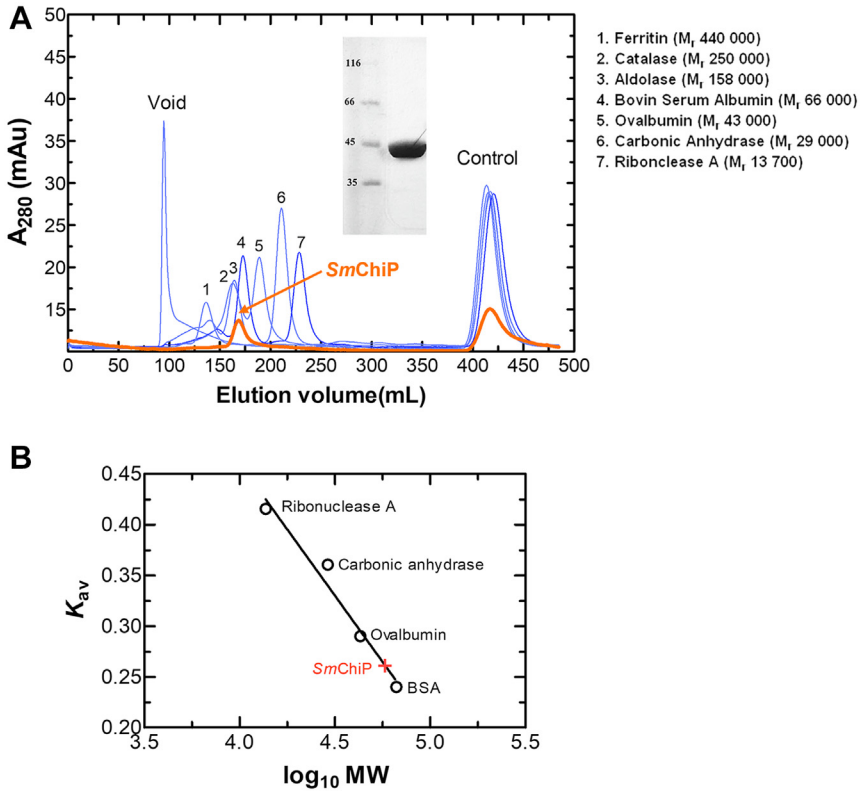

Figure 3. Molecular weight determination by size-exclusion chromatography. *A*, standard proteins and *Sm*ChiP were resolved on a HiPrep 16/60 Sephacryl S-200 HR prepacked column under the conditions described in the text. *B*, the molecular weight of *Sm*ChiP was estimated from the plot of the distribution coefficient (K_{av}) *versus* $\log_{10}$ MW of four well-resolved standard proteins: ribonuclease, carbonic anhydrase, ovalbumin, and BSA. Control peaks were DNP-lysine, which was applied to determine the total volume of the GF column. The *inset* shows migration of *Sm*ChiP on SDS-PAGE, in comparison with that of the standard proteins. The protein bands were stained with Coomassie blue G-250 and photographed in monochrome. GF, gel filtration; *Sm*ChiP, *Serratia marces*cens chitoporin.

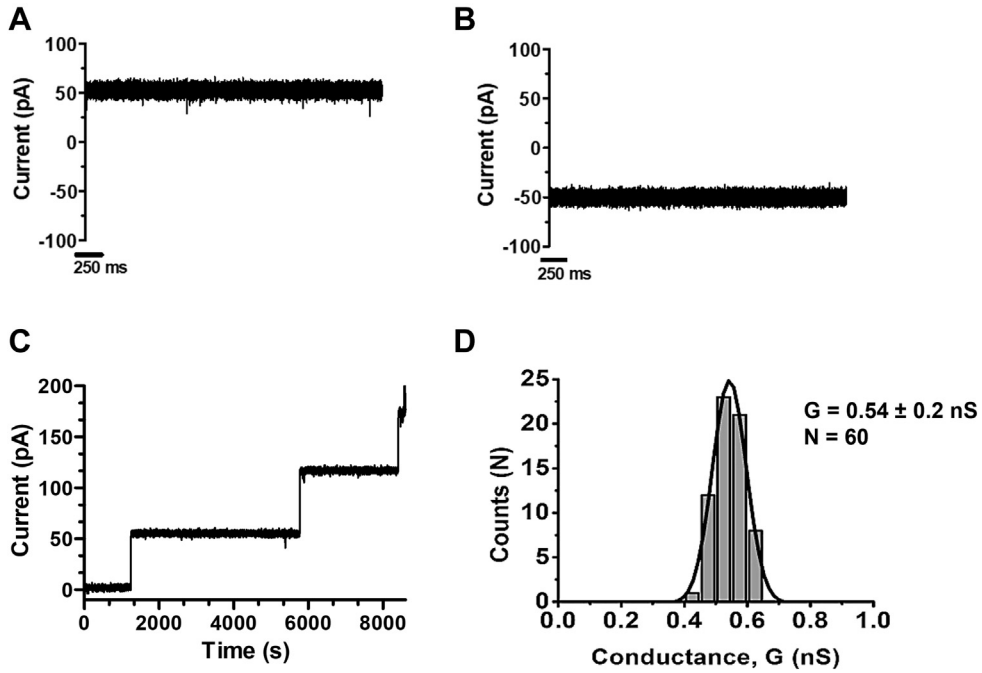

Figure 4. Pore-forming properties of *Sm*ChiP in artificial lipid membranes. Lipid bilayer measurements (BLM) were formed by a lowering-and-raising technique, using 5 mg ml^{-1} DPhPC bathed on either side with 1 M KCl in 20 mM Hepes, pH 7.4. The protein was always added to the *cis* side of the chamber. *A*, current trace at +100 mV, (*B*) current trace at −100 mV, and (*C*) multiple channel insertion. *D*, histogram analysis of channel conductance observed from 60 independent channel insertions. The distribution of the conductance profile was fitted to a Gaussian curve by Clampfit *v*.10.4. DPhPC, 1,2-diphytanoyl-sn-glycero-3-phosphatidylcholine; *Sm*ChiP, *Serratia marces*cens chitoporin.

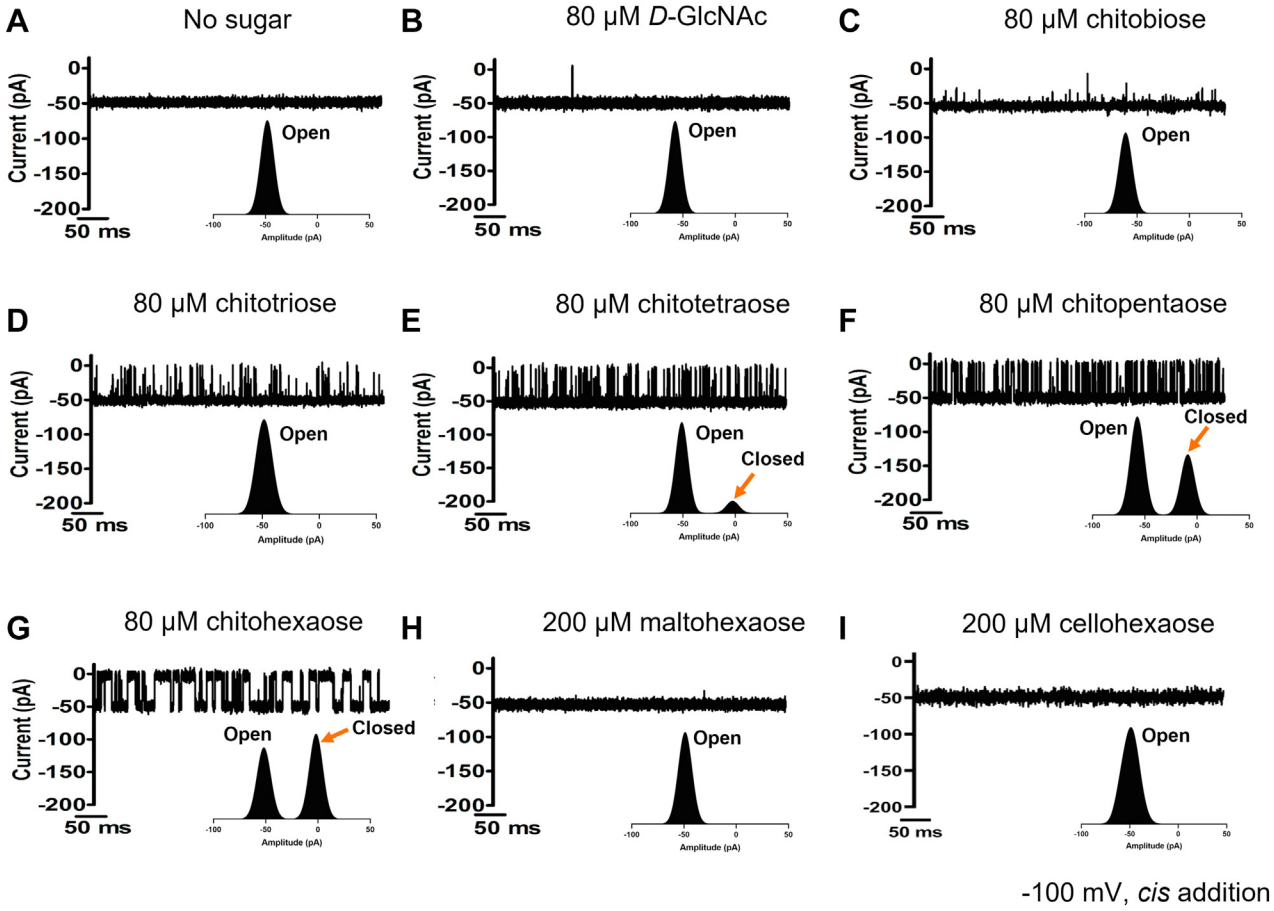

Figure 5. Channel specificity. Ion current fluctuations were monitored for 120 s at applied potentials of ±100 mV when sugar was added on either the *cis* or the *trans* side. Here, only current traces for 500 ms at −100 mV, with *cis* side addition, are shown. *A*, a fully open state of *Sm*ChiP before sugar addition. *B*, *D*-GlcNAc (*N*-acetylglucosamine), (*C*) chitobiose, (*D*) chitotriose, (*E*) chitotetraose, (*F*) chitopentaose, and (*G*) chitohexaose, added on the *cis* side of the chamber to a final concentration of 80 μM. *H* and *I*, are control recordings with maltohexaose and cellohexaose (each 200 μM), respectively. The histogram below each trace shows the distribution of the channel between open and closed (*red arrows*) state.

(in Fig. 5 a trace of length 500-ms is shown). The addition of 80 μM *D*-GlcNAc (Fig. 5*B*) on either side of the chamber did not disturb the ion flow, while the addition of chitobiose at the same concentration (Fig. 5*C*) caused slight flickering of the current trace. Disturbance of the ion flow was seen when the channel was exposed to chitotriose. Figure 5*D* shows that the sugar molecules occluded the channel, causing short-lived blocking events throughout the recording time. The addition of chitotetraose (Fig. 5*E*) also yielded frequent, full blocking events. A similar blocking pattern was observed with chitopentaose, with more blocking events than were detected with chitotriose and chitotetraose (Fig. 5*F*). In the case of chitohexaose, although a lower number of blocking events was seen, they were full and long-lived (Fig. 5*G*). In contrast, addition of a nearly three-fold higher concentration (200 μM) of maltohexaose (Fig. 5*H*) or cellohexaose (Fig. 5*I*) did not interfere with ion current traces from *Sm*ChiP. The average residence time (τ_c) for channel blocking by chitotriose cannot be evaluated with confidence because of the limit of time resolution of our BLM instrument (<100 μS). However, the residence times for chitotetraose, chitopentaose, and chitohexaose were estimated to be 0.3, 1.3, and 6.0 ms, respectively.

Histogram analysis confirmed the blocking characteristics of individual sugar species (Fig. 5, *A–I*, insets). *D*-GlcNAc, chitobiose, and chitotriose (Fig. 5, *B–D*, insets) did not alter the amplitude of the ionic current, which corresponded to the fully 'open' state of the channel (50 pA at +100 mV). On the other hand, transient blockings caused a discrete reduction of the ion current to zero when 80 μM of chitotetraose, chitopentaose, or chitohexaose was added. The fraction of the porin at zero current (labeled 'closed') increased as the chain length increased, indicating that long-chain chitooligosaccharides induced more complete blocking of the protein subunits (Fig. 5, *E–G*, insets).

Bulk permeation of small monosaccharides and chitooligosaccharides through SmChiP

Liposome swelling assays were carried out to examine the permeation of bulk sugars through the *Sm*ChiP-reconstituted proteoliposomes. Figure 6*A* shows the swelling rate with small sugar molecules of molecular weights 180 to 600 Da. The permeation rate of the tested sugar was estimated relative to that of the smallest sugar (*D*-arabinose, MW = 150), which was set to 100%. The isotonic concentration was determined to be

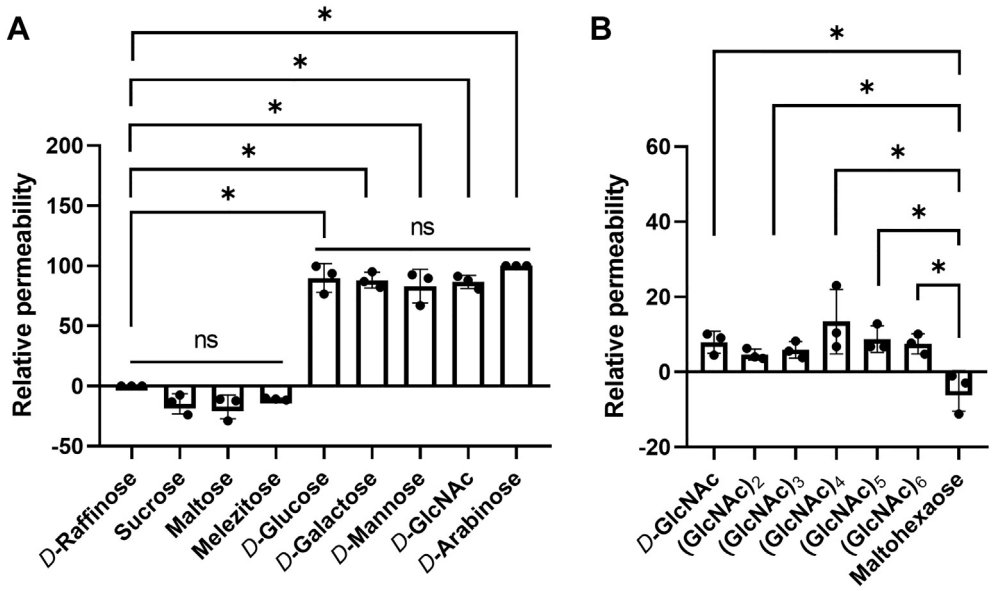

Figure 6. Proteoliposome swelling assays. *D*-raffinose was used to determine the isotonic concentration, *i.e.*, the concentration of solute that produced no change in absorbance at 500 nm of the proteoliposome suspension over 60 s, and the swelling rate in *L*-arabinose was set to 100% to normalize swelling rates. The permeability of the channel was assumed to be proportional to the swelling rate. *A*, permeation of different types of small sugars (monosaccharides and disaccharides, 70 mM) through *Sm*ChiP reconstituted in liposomes. *B*, permeation of chitooligosaccharides (2 mM) through *Sm*ChiP. Values are means ± SD obtained from three independent sets of experiments. *Circles* on the bar graphs represent individual values. Statistical analysis was performed using One-way ANOVA, available in Prism. Significant differences are shown by *asterisks* (*) and set at $0.001 < p < 0.05$. *Sm*ChiP, *Serratia marcescens* chitoporin.

70 mM, using the impermeant sugar raffinose. All monosaccharides, including *D*-glucose, *D*-galactose, and *D*-mannose (all of MW = 180 kDa) and *D*-GlcNAc (MW = 222 Da), permeated the liposomes at relative rates of nearly 100%, while the disaccharides *D*-sucrose (MW = 342), *D*-maltose (MW = 360), and *D*-melezitose (MW = 522) were completely impermeant, reflecting a pore constriction limit of <300 Da. The permeation rates of different chitooligosaccharides were also tested. Figure 6*B* suggests that all chitooligosaccharides could permeate through the liposomes, even at a concentration as low as 2.5 mM. Chitotetraose, chitopentaose, and chitohexaose had slightly higher permeation rates than chitobiose and chitotriose. However, maltohexaose did not permeate through *Sm*ChiP at all.

Substrate binding affinity of Sm*ChiP*

Isothermal microcalorimetric (ITC) titrations were carried out with *Sm*ChiP in solution with two preferred substrates (chitohexaose and chitopentaose) and were compared to the data with a nonchitin oligosaccharide (maltohexaose).

Figure 7*A* shows the ITC thermograms obtained from titrating chitohexaose to *Sm*ChiP, and Figure 7*B* shows the theoretical fit of the normalized, integrated heat using a one-site binding model available in MicroCal PEAQ-ITC Analysis Software. Figure 7, *C* and *D* show the isothermal binding thermogram and the corresponding curve fit for chitopentaose. The equilibrium dissociation constant (K_d) was estimated to be 17 ± 0.6 μM for chitohexaose and 23 ± 2.0 μM for chitopentaose. Figure 7*E* is the isothermal titration profile of maltohexaose, showing no heat release (<0.1 μcal per injection) and yielding no integrated heat change (Fig. 7*F*), as a result of no binding.

Growth of S. marcescens *on different carbon sources*

S. marcescens was grown on M9 minimal medium (MM) supplemented with three different carbon sources: *D*-glucose, a chitooligosaccharide mixture, and chitosan oligomers, and the growth was monitored at different time points from 0 to 96 h. Figure 8 shows the rapid growth of *S. marcescens* during the log phase of incubation (within 24 h), when *D*-glucose and chitin oligomers were used as the carbon source. The growth rate after entering the stationary phase declined less slowly with the cells grown on chitooligosaccharides than on *D*-glucose. *S. marcescens* could barely grow on MM supplemented with chitosan oligomers and was unable to grow on MM with no supplementary carbon source.

Discussion

The *chiP* gene encoding *Sm*ChiP from *S. marcescens* 2170 was first identified as part of the *ybfMN-ctp* gene cluster. Later, this was referred to as the *chiPQ-ctb* cluster (40). The same study also generated the *S. marcescens* mutants lacking the *chiP*, *chiX*, and *chiQ* genes. Deletions of these target genes affected the growth of the bacterium. In particular, the △*chiP* mutant showed significantly lower ability to grow on medium supplemented with colloidal chitin and $(GlcNAc)_2$, and no growth on medium containing $(GlcNAc)_3$. Subsequent studies demonstrated that the *chiX* small RNA controlled the expression of chitin-degrading enzymes (chitinases, chitobiase, and *N*-acetylglucosaminidase), chitin-binding protein (CBP21)

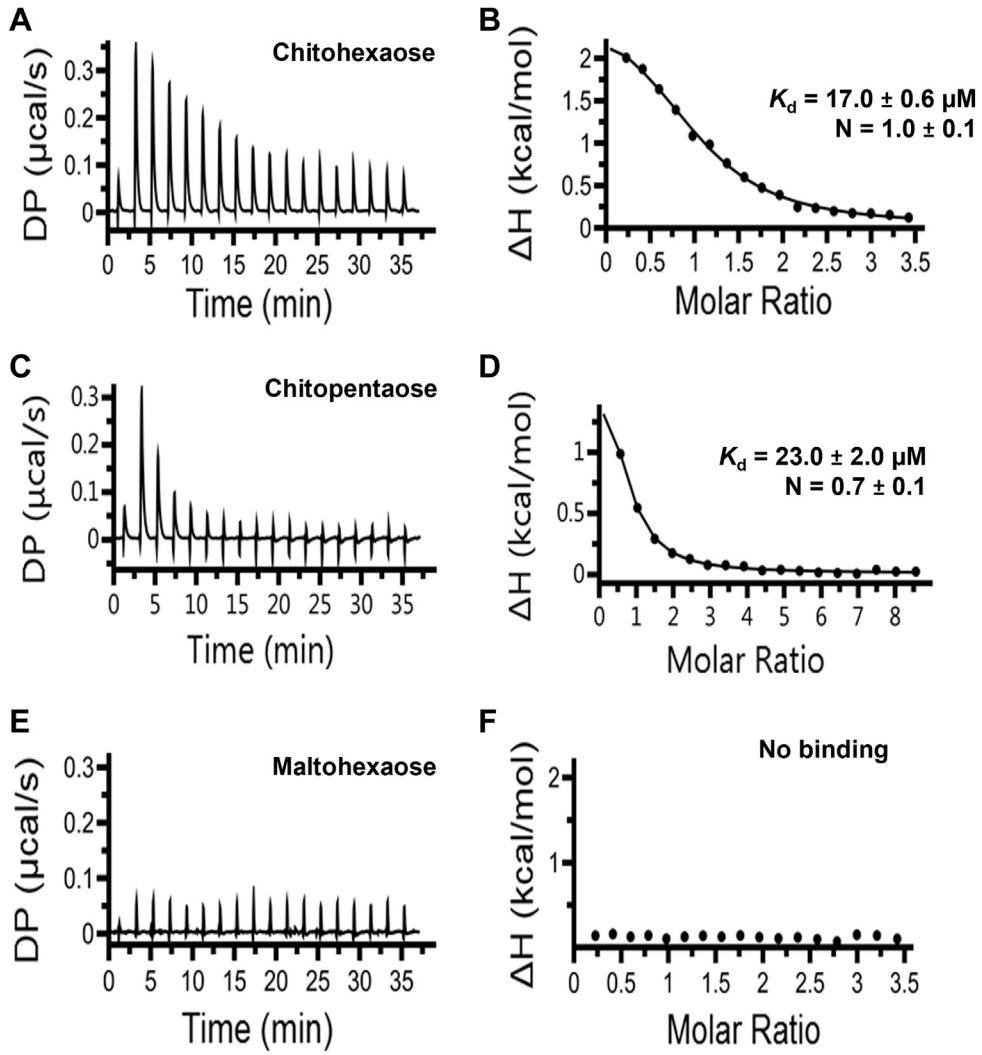

Figure 7. Binding studies of SmChiP with three oligosaccharides. Microcalorimetric titrations of *Sm*ChiP with oligosaccharides, showing ITC profiles corresponding to the binding of (*A*) chitohexaose, (*C*) chitopentaose, and (*E*) maltohexaose to *Sm*ChiP. *B*, integrated curve fitting for heat of binding of chitohexaose, (*D*) chitopentaose and (*F*) maltohexaose. ITC, isothermal microcalorimetric; *Sm*ChiP, *Serratia marce*scens chitoporin.

(41), and a chitooligosaccharide-transporting porin (later named *Sm*ChiP) (33, 40). Nonetheless, no detailed functional and structural characterization of *Sm*ChiP has been reported to date. In the present study, we heterologously expressed *Sm*ChiP in the *E. coli* system. The pore-forming properties of *Sm*ChiP in lipid membranes were elucidated at the single-molecule level. In contrast to the well-characterized trimeric *Vh*ChiP from *V. campbellii* (formerly *V. harveyi*) (33, 38, 40) and *Vc*ChiP from *Vibrio cholerae* (34), *Sm*ChiP was shown to be a member of the class of monomeric porins, like the closely related *Ec*ChiP (35). Although most porins form trimers, a few were shown to be monomeric, including *Pseudomonas aeruginosa* OCCDs and OCCKs (formerly referred as OprD porins) (42, 43) and *E. coli* OmpG (44).

Bulk permeability of different sugars through *Sm*ChiP, as determined by a liposome swelling assay, provided an estimated size exclusion limit of about 300 Da. In our study, only monosaccharides were able to pass through the protein pore by general diffusion. *Sm*ChiP exhibited clear substrate specificity, being completely impermeable to nonchitin oligosaccharides. However, BLM results showed that chitobiose and longer-chain chitooligosaccharides (chitotriose, -tetraose, -pentaose and -hexaose) could permeate through *Sm*ChiP, despite their MWs exceeding its size exclusion limit. We recently showed that the C_2-acetamido functionality on the GlcNAc units of the chitooligosaccharide chain served as a molecular footprint for sugar-channel recognition (45). *Sm*ChiP was shown to have no binding affinity for chitosan oligomers (deacetylated chitooligosaccharides), since these sugars lack the C_2-acetamido functional groups. Our thermodynamic data obtained from ITC experiments confirmed that the binding affinity for the most highly preferred substrate, chitohexaose (K_d = 17 µM or K = 60,000 M^{-1}) was 4.2-fold and 8.4-fold lower than for chitohexaose binding to *Ec*ChiP (K = 250,000 M^{-1}) (35) and to *Vh*ChiP (K = 500,000 M^{-1}), respectively. The ITC data confirmed that *Sm*ChiP had weaker substrate-binding affinity than *Ec*ChiP (35) and *Vh*ChiP (40).

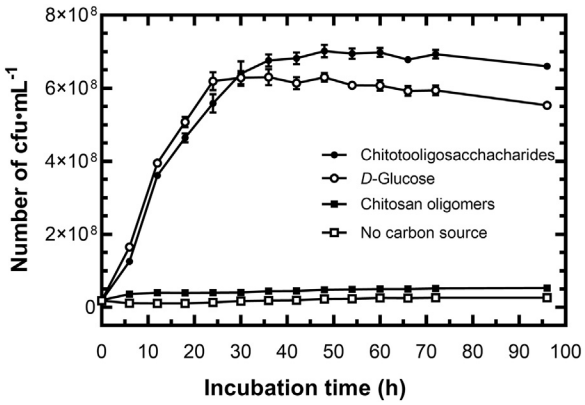

Figure 8. Growth of *S. marcescens* on various carbon sources. *S. marcescens* were grown on M9 minimal medium supplemented with 0.5% (*w/v*) chitooligosaccharide mixture, *D*-glucose, or chitosan oligomers. The growth rate was monitored at different time points of incubation up to 96 h, at 26 °C.

Single-channel recordings suggested that *Sm*ChiP could form a highly stable channel over a wide range of applied external potentials (±25 to ±150 mV), with neither gating nor stepwise closure. The average single-channel conductance of *Sm*ChiP (G = 0.5 ± 0.2 nS) was approximately one-third of the mean conductance reported for trimeric *Vh*ChiP (G = 1.8 ± 0.3 nS) (40), which confirmed the monomeric state of *Sm*ChiP. Cell growth assays showed that *S. marcescens* could grow on chitin oligosaccharides, owing to its ability to digest chitinous materials and transport the degradation products through *Sm*ChiP into the cell.

Figure 9 is a schematic illustration of chitin processing by the OM and inner membrane (IM) of *S. marcescens*, suggested by Watanabe *et al.* (22, 23). Chitin is initially digested by chitinases, generating chitooligosaccharides of various lengths as the initial products, and finally further generating $(GlcNAc)_2$ as the major product (dark arrow), along with the monosaccharide (*D*-GlcNAc) as a minor product (dashed arrow). The chitin degradation products enter the periplasm by two possible routes: $(GlcNAc)_2$ and chitooligosaccharides through *Sm*ChiP and GlcNAc through a general diffusion porin. $(GlcNAc)_2$ in the periplasm was suggested to be transported further through the IM by a specific $(GlcNAc)_2$-specific enzyme IIC, encoded by the *chb* operon (22). On the other hand, GlcNAc is further transported through the IM by a GlcNAc-specific phosphoenolpyruvate:carbohydrate phosphotransferase system transporter. $(GlcNAc)_2$ and GlcNAc entering the cytoplasm *via* phosphoenolpyruvate:carbohydrate phosphotransferase system are phosphorylated during transport to $(GlcNAc)_2$-P and GlcNAc-6P, which are further metabolized in the cytoplasm (46).

In conclusion, this study elucidates the physiological function of a chitooligosaccharide-specific porin from the *Serratia* system and provides an understanding of how the *Serratia* bacteria can utilize chitin as their carbon source. Given that *Sm*ChiP is the molecular gateway for nutrient uptake, it may serve as an excellent protein target for the strategic design of effective antimicrobial agents with a novel mode of action, such as the chemoenzymatic synthesis of chitooligosaccharide-based compounds that can inhibit *Serratia* infections.

Experimental procedures

Bacterial strains and vectors

The pET23a(+) expression vector, carrying the *S. marcescens ChiP* gene, was obtained from GenScript USA Inc. *E. coli* strain DH5α, used for plasmid preparations, was obtained from Invitrogen (Gibthai Company, Ltd). *E. coli* BL21 (DE3) Omp8 Rosetta strain, lacking the major endogenous Omps (OmpF, OmpC, OmpA, and LamB) was a gift from Professor Dr Roland Benz, Jacobs University Bremen, Germany. Chitooligosaccharides were purchased from Dextra Laboratories and Megazyme.

Structure-based sequence alignment and AlphaFold2 structural prediction

Structure-based sequence alignment was performed for representative ChiPs from *S. marcescens* (*Sm*ChiP; protein id: A0A0PBS3), *E. coli* (*Ec*ChiP, protein id: P75733), *V. cholerae* (*Vc*ChiP, protein id: Q9KTD0), and *V. harveyi*, now classified as *V. campbellii* (*Vh*ChiP, protein id: L0RYU0). The corresponding sequences were retrieved from the UniProtKB

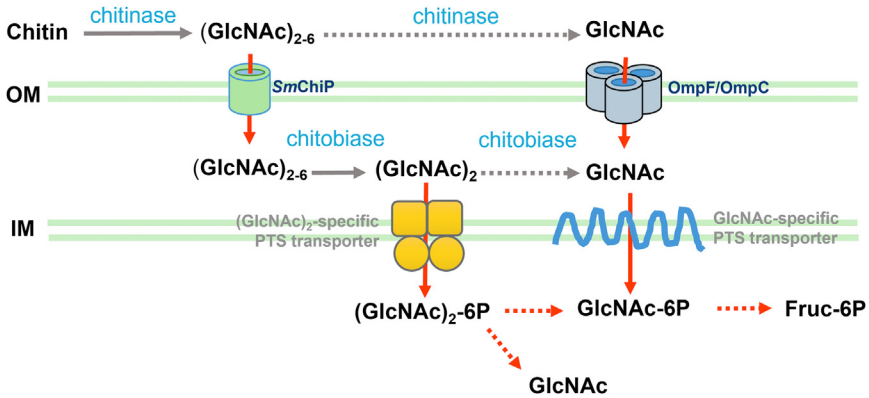

Figure 9. Chitin utilization by *S. marcescens*. GlcNAc and $(GlcNAc)_{2-6}$ are chitooligosaccharides generated by the cleavage of chitin by chitinase. GlcNAcase is a periplasmic β-N-acetylglucosaminidase and GlcN is glucosamine. *Gray arrows* indicate the main enzymic route, while *dashed arrows* indicate minor enzymic routes. *Red arrows* indicate translocation steps. IM, inner membrane; OM, outer membrane; PTS, phosphoenolpyruvate:carbohydrate phosphotransferase system.

database (https://www.uniprot.org/uniprot/), aligned by Muscle alignment (47) and displayed in Jalview *v.* 2.11.2.1. The 2D structural elements of monomeric *Sm*ChiP were constructed from AlphaFold2 (https://alphafold.ebi.ac.uk/), while the 2D structural elements of trimeric *Vh*ChiP were constructed from the crystal structure of the native form (PDB id: 5MDO).

Recombinant expression, cell wall extraction, and protein purification

Cloning of the *chiP* gene encoding *Sm*ChiP and purification of the recombinant protein were described in our previous report (31). Briefly, the overnight culture of transformed cells was transferred to Luria-Bertani (LB) broth containing 100 μg ml^{-1} ampicillin and 25 μg ml^{-1} kanamycin and grown at 25 + 1 °C until A_{600} ∼0.6 to 0.8. *Sm*ChiP expression was then induced with 0.5 mM of isopropyl thio-*β*-D-galactoside for 6 h at 37 °C. For protein purification, the cell pellet, collected after centrifugation and resuspended in lysis buffer (20 mM Tris-HCl pH 8.0, 2.5 mM $MgCl_2$, 0.1 mM $CaCl_2$), containing 10 μg ml^{-1} RNase A and 10 μg ml^{-1} DNase I, was subjected to high-speed ultrasonic homogenization (Emulsi-Flex-C3). Cell walls were extracted by incubating the crude extract in 2% (*w/v*) SDS solution at 50 °C for 60 min. After centrifugation at 100,000*g* at 4 °C for 1 h, the cell wall faction (pellet) was extracted twice with 2.5% (*v/v*) octyl-POE (*n*-octylpolyoxyethylene; ALEXIS Biochemicals). After centrifugation at the same speed, the supernatant containing OM-expressed *Sm*ChiP was dialyzed thoroughly against 20 mM potassium phosphate buffer, pH 7.4, containing 0.05% (*v/v*) lauryldimethylamine oxide (Sigma-Aldrich Pte Ltd), and purified by ion-exchange chromatography on a Hitrap Q HP prepacked column (1 cm Ø × 5 cm L), followed by gel filtration chromatography on a HiPrep 16/60 Sephacryl S-200 High Resolution column (GE Healthcare Life Sciences). The purity of the *Sm*ChiP fractions obtained after the gel filtration step was verified by SDS-PAGE, and the protein concentration of the purified *Sm*ChiP was estimated using the Novagen BCA protein assay kit (EMD Chemicals Inc)

Molecular weight determination of native Sm*ChiP*

The molecular weight of *Sm*ChiP in its native state was determined by size-exclusion chromatography. Standard proteins of known molecular weight were resolved on a HiPrep 16/60 Sephacryl S-200 HR prepacked column (GE Healthcare Life Sciences) under the conditions described above. Dextran-2000 was used to obtain the void volume (V_0), while *DNP*-lysine was used to calculate the volume of the stationary phase (V_i). With the elution volume of each protein sample denoted V_e, the elution of the protein sample is described by the distribution coefficient (K_{av}) defined in Equation 1 (48):

$$K_{av} = \frac{V_e - V_o}{V_i} \quad (1)$$

A calibration curve was created by plotting K_{av} *versus* logarithmic values of the corresponding molecular weights of the standard proteins and was used to estimate the molecular weight of *Sm*ChiP. The standard proteins used in this experiment were ferritin (440 kDa), catalase (250 kDa), aldolase (158 kDa), bovine serum albumin (66 kDa), ovalbumin (43 kDa), carbonic anhydrase (29 kDa), and ribonuclease A (13.7 kDa).

Single-channel electrophysiology

Montal-Mueller type solvent-free bilayer (49) formation was performed using 5 mg ml^{-1} 1,2-diphytanoyl-sn-glycero-3-phosphatidylcholine (Avanti Polar Lipids) in n-pentane. First, a 25-mm-thick Teflon film with an aperture of 50 to 100 mm was sandwiched between the two chambers of a cuvette, and the aperture was prepainted with a few microliters of 1% (*v/v*) hexadecane in hexane. The chambers were filled with 1 M KCl in 20 mM Hepes, pH 7.4, and BLM experiments were carried out at 25 °C. A planar bilayer was formed across the aperture by lowering and raising the liquid level (33). Ionic currents were detected using Ag/AgCl electrodes, with the reference electrode connected to the *cis* side of the membrane (ground) and the working electrode connected to the head-stage of an Axopatch 200B amplifier (Axon Instruments). Single-channel measurements were performed in the voltage clamp mode and digitized using the Axon Digidata 1550 digitizer, and the data acquisition was performed using Clampex software (Axon Instruments). Using a low-pass Bessel filter with a sampling frequency of 50 kHz, the traces obtained were filtered at 10 kHz. Single channel analyses were performed using Clampfit software (all from Molecular Devices). Single protein channels were reconstituted in lipid, and fully open channels of *Sm*ChiP were titrated with discrete concentrations of chitooligosaccharides at the *cis* or *trans* side of the chamber. Fluctuations of ion flow produced by sugar diffusion through the inserted channel were usually recorded for 2 min at different transmembrane potentials of ±25 to ±100 mV. Multiple channel insertion experiments were operated with a patch-clamp amplifier connected to a two-electrode bilayer head-stage (PC-ONE plus PC-ONE-50; Dagan Corp) together with an A/D converter (LIH 1600, HEKA Elektronik) that was operated using PULSE program (HEKA Elektronik).

Liposome swelling experiments

The *Sm*ChiP-reconstituted proteoliposomes were prepared as described elsewhere (35, 50). Soybean L-α-phosphatidylcholine [20 mg ml^{-1}, (Sigma) freshly prepared in chloroform] was used to form multilamellar liposomes. For the preparation of proteoliposomes, 200 ng of *Sm*ChiP was reconstituted into 200 μl of the liposome suspension by sonication, and then 17% (*w/v*) dextran (40 kDa) was entrapped in the proteoliposomes. *D*-Raffinose solutions were prepared in 20 mM potassium phosphate buffer, pH 7.4, to obtain concentrations of 40, 50, 60, and 70 mM for determination of the isotonic solute concentration. This value was then used for the adjustment of the isotonic concentration for other solutes. To carry out a liposome-swelling assay, 25 μl of the proteoliposome suspension was added to 600 μl of sugar solution, and changes in

absorbance at 500 nm were monitored immediately. The apparent absorbance change over the first 60 s was used to estimate the swelling rate (s^{-1}) following the equation $\Phi = (1/A_i)dA/dt$ in which Φ is the swelling rate, A_i is the initial absorbance, and dA/dt is the rate of absorbance change during the first 60 s. The swelling rate for each sugar was normalized by setting the rate of *L*-arabinose (150 Da) to 100%. The values presented are averages from three independent determinations. Protein-free liposomes and proteoliposomes without sugars were used as negative controls. The sugars tested were *D*-glucose (180 Da), *D*-mannose (180 Da), *D*-galactose (180 Da), *N*-acetylglucosamine (GlcNAc) (221 Da), *D*-sucrose (342 Da), *D*-melezitose (522 Da), $GlcNAc_2$ (424 Da), $GlcNAc_3$ (628 Da), $GlcNAc_4$ (830 Da), $GlcNAc_5$ (1034 Da), $GlcNAc_6$ (1237 Da), and maltodextrins.

Chitooligosaccharide-induced growth of S. marcescens

S. marcescens was streaked onto LB agar plates, then incubated at 26 °C overnight. A single colony was picked and inoculated into LB medium for gentle shaking at 26 °C overnight. The bacterial cells were grown in M9 minimal medium (26 mM Na_2HPO_4, 22 mM KH_2PO_4, 19 mM NH_4Cl, 2 mM $MgSO_4$, 0.1 mM $CaCl_2$, and 8.6 mM NaCl), supplemented with various carbon sources (*D*-glucose, chitosan oligomers or chitooligosaccharides), all at 0.5% (*w/v*). Cells (150 µl) were collected to measure A_{600} in a microtiter plate during each time course (0–96 h). Cell growth was monitored with a microplate reader model MULTISKAN Sky (Thermo Fisher Scientific). The number of cells ($cfu.ml^{-1}$) was calculated from A_{600} (0.1 A_{600} = 1 × 10^8 $cfu.ml^{-1}$) (51).

Data availability

The BLM and ITC datasets for this study can be found in the following URL link: https://drive.google.com/drive/folders/1qh5qDiOhLt0-c18cgT41XgZ42AY8jyA4.

Acknowledgments—We would like to acknowledge the help of Dr David Apps, University of Edinburgh, Scotland for critical readings of the manuscript. We would also like to thank Professor Mathias Winterhalter, Jacobs University Bremen, Germany, for providing the BLM setup for single channel measurements.

Author contributions—H. S. M. S., S. K., and R. A. methodology; H. S. M. S., S. K., and R. A. software; H. S. M. S., S. K., and R. A. data curation; H. S. M. S., S. K., and R. A. writing-original draft; H. S. M. S., S. K., and R. A. visualization; H. S. M. S., S. K., and R. A. investigation; H. S. M. S. formal analysis; T. W. and W. S. conceptualization; T. W. and W. S. writing-review and editing; W. S. supervision; W. S. validation.

Funding and additional information—This research was funded by Thailand Science Research and Innovation (TSRI) and Vidyasirimedhi Institute of Science and Technology (VISTEC) (BRG610008). H. S. M. S. received PhD funding from Suranaree University of Technology (SUT) through an OGRG grant.

Conflict of interest—The authors declare that they have no conflicts of interest with the contents of this article.

Abbreviations—The abbreviations used are: ChiPs, chitoporins; GlcNAc, *N*-acetylglucosamine; $(GlcNAc)_2$, chitobiose; $(GlcNAc)_n$, n >2, chitooligosaccharides; IM, inner membrane; ITC, isothermal microcalorimetric; K_d, equilibrium dissociation constant (µM); MM, M9 minimal medium; OM, outer membrane; *Sm*ChiP, *Serratia marcescens* chitoporin.

References

1. Mahlen, S. D. (2011) *Serratia* infections: from military experiments to current practice. *Clin. Microbiol. Rev.* **24**, 755–791
2. Yoon, H. J., Choi, J. Y., Park, Y. S., Kim, C. O., Kim, J. M., Yong, D. E., *et al.* (2005) Outbreaks of Serratia marcescens bacteriuria in a neurosurgical intensive care unit of a tertiary care teaching hospital: a clinical, epidemiologic, and laboratory perspective. *Am. J. Infect. Control* **33**, 595–601
3. Voelz, A., Müller, A., Gillen, J., Le, C., Dresbach, T., Engelhart, S., *et al.* (2009) Outbreaks of Serratia marcescens in neonatal and pediatric intensive care units: clinical aspects, risk factors and management. *Int. J. Hyg. Environ. Health* **213**, 79–87
4. Jones, R. N. (2010) Microbial etiologies of hospital-acquired bacterial pneumonia and ventilator-associated bacterial pneumonia. *Clin. Infect. Dis.* **51**, S81–S87
5. van der Vorm, E. R., and Woldring-Zwaan, C. (2002) Source, carriers, and management of a *Serratia marcescens* outbreak on a pulmonary unit. *J. Hosp. Infect.* **52**, 263–267
6. Aronson, L. C., and Alderman, S. I. (1943) The occurrence and bacteriological characteristics of *S. marcescens* from a case of meningitis. *J. Bacteriol.* **43**, 261–267
7. Rabinowitz, K., and Schiffrin, R. (1952) A ward contamination by *Serratia marcescens*. *Acta Med. Orient.* **11**, 181–184
8. Kawecki, D., Kwiatkowski, A., Sawicka-Grzelak, A., Durlik, M., Paczek, L., Chmura, A., *et al.* (2011) Urinary tract infections in the early post-transplant period after kidney transplantation: etiologic agents and their susceptibility. *Transplant. Proc.* **43**, 2991–2993
9. Nikaido, H. (1989) Outer membrane barrier as a mechanism of antimicrobial resistance. *Antimicrob. Agents Chemother.* **33**, 1831–1836
10. Stock, I., Grueger, T., and Wiedemann, B. (2003) Natural antibiotic susceptibility of strains of *Serratia marcescens* and the *S. liquefaciens* complex: *S. liquefaciens* sensu stricto, *S. proteamaculans* and *S. grimesii*. *Int. J. Antimicrob. Agents* **22**, 35–47
11. Arakawa, Y. (2020) Systematic research to overcome newly emerged multidrug-resistant bacteria. *Microbiol. Immunol.* **64**, 231–251
12. Cooksey, R. C., Thorne, G. M., and Farrar, W. E., Jr. (1976) R factor-mediated antibiotic resistance in *Serratia marcescens*. *Antimicrob. Agents Chemother.* **10**, 123–127
13. Shirshikova, T. V., Sierra-Bakhshi, C. G., Kamaletdinova, L. K., Matrosova, L. E., Khabipova, N. N., Evtugyn, V. G., *et al.* (2021) The ABC-type efflux pump MacAB is involved in protection of *Serratia marcescens* against aminoglycoside antibiotics, polymyxins, and oxidative stress. *mSphere* **6**, e00033-21
14. Hall-Stoodley, L., Costerton, J. W., and Stoodley, P. (2004) Bacterial biofilms: from the natural environment to infectious diseases. *Nat. Rev. Microbiol.* **2**, 95–108
15. Satpathy, S., Sen, S. K., Pattanaik, S., and Raut, S. (2016) Review on bacterial biofilm: an universal cause of contamination. *Biocatal. Agric. Biotechnol.* **7**, 56–66
16. Srinivasan, R., Devi, K. R., Kannappan, A., Pandian, S. K., and Ravi, A. V. (2016) *Piper betle* and its bioactive metabolite phytol mitigates quorum sensing mediated virulence factors and biofilm of nosocomial pathogen *Serratia marcescens in vitro*. *J. Ethnopharmacol.* **193**, 592–603
17. Ray, C., Shenoy, A. T., Orihuela, C. J., and González-Juarbe, N. (2017) Killing of *Serratia marcescens* biofilms with chloramphenicol. *Ann. Clin. Microbiol. Antimicrob.* **16**, 19
18. Jacoby, G. A. (2009) AmpC beta-lactamases. *Clin. Microbiol. Rev.* **22**, 161–182

19. Bes, T., Nagano, D., Martins, R., Marchi, A. P., Perdigão-Neto, L., Higashino, H., *et al.* (2021) Bloodstream infections caused by *Klebsiella pneumoniae* and *Serratia marcescens* isolates co-harboring NDM-1 and KPC-2. *Ann. Clin. Microbiol. Antimicrob.* **20**, 57
20. Harris, P. N., and Ferguson, J. K. (2012) Antibiotic therapy for inducible AmpC beta-lactamase-producing Gram-negative bacilli: what are the alternatives to carbapenems, quinolones and aminoglycosides? *Int. J. Antimicrob. Agents* **40**, 297–305
21. Vaaje-Kolstad, G., Horn, S. J., Sørlie, M., and Eijsink, V. G. H. (2013) The chitinolytic machinery of *Serratia marcescens*–a model system for enzymatic degradation of recalcitrant polysaccharides. *FEBS J.* **280**, 3028–3049
22. Uchiyama, T., Kaneko, R., Yamaguchi, J., Inoue, A., Yanagida, T., Nikaidou, N., *et al.* (2003) Uptake of *N,N′*-diacetylchitobiose [$(GlcNAc)_2$] via the phosphotransferase system is essential for chitinase production by *Serratia marcescens* 2170. *J. Bacteriol.* **185**, 1776–1782
23. Suzuki, K., Shimizu, M., Sasaki, N., Ogawa, C., Minami, H., Sugimoto, H., *et al.* (2016) Regulation of the chitin degradation and utilization system by the ChiX small RNA in *Serratia marcescens* 2170. *Biosci. Biotechnol. Biochem.* **80**, 376–385
24. Monreal, J., and Reese, E. T. (1969) The chitinase of *Serratia marcescens*. *Can. J. Microbiol.* **15**, 689–696
25. Watanabe, T., Kimura, K., Sumiya, T., Nikaidou, N., Suzuki, K., Suzuki, M., *et al.* (1997) Genetic analysis of the chitinase system of *Serratia marcescens* 2170. *J. Bacteriol.* **179**, 7111–7117
26. Suzuki, K., Sugawara, N., Suzuki, M., Uchiyama, T., Katouno, F., Nikaidou, N., *et al.* (2002) Chitinases A, B, and C1 of *Serratia marcescens* 2170 produced by recombinant *Escherichia coli*: enzymatic properties and synergism on chitin degradation. *Biosci. Biotechnol. Biochem.* **66**, 1075–1083
27. Takanao, S., Honma, S., Miura, T., Ogawa, C., Sugimoto, H., Suzuki, K., *et al.* (2014) Construction and basic characterization of deletion mutants of the genes involved in chitin utilization by *Serratia marcescens* 2170. *Biosci. Biotechnol. Biochem.* **78**, 524–532
28. Synstad, B., Vaaje-Kolstad, G., Cederkvist, F. H., Saua, S. F., Horn, S. J., Eijsink, V. G. H., *et al.* (2008) Expression and characterization of endochitinase C from *Serratia marcescens* BJL200 and its purification by a one-step general chitinase purification method. *Biosci. Biotechnol. Biochem.* **72**, 715–723
29. Sánchez, L., Ruiz, N., Leranoz, S., Viñas, M., and Puig, M. (1997) The role of outer membrane in *Serratia marcescens* intrinsic resistance to antibiotics. *Microbiologia* **13**, 315–320
30. Begic, S., and Worobec, E. A. (2006) Regulation of *Serratia marcescens ompF* and *ompC* porin genes in response to osmotic stress, salicylate, temperature and pH. *Microbiology (Reading)* **152**, 485–491
31. Amornloetwattana, R., Robinson, R. C., Soysa, H. S. M., van den Berg, B., and Suginta, W. (2020) Chitoporin from *Serratia marcescens*: recombinant expression, purification and crystallization. *Acta Crystallogr. F Struct. Biol. Commun.* **76**, 536–543
32. Keyhani, N. O., Li, X. B., and Roseman, S. (2000) Chitin catabolism in the marine bacterium *Vibrio furnissii*. Identification and molecular cloning of a chitoporin. *J. Biol. Chem.* **275**, 33068–33076
33. Suginta, W., Chumjan, W., Mahendran, K. R., Janning, P., Schulte, A., and Winterhalter, M. (2013) Molecular uptake of chitooligosaccharides through chitoporin from the marine bacterium *Vibrio harveyi*. *PLoS One* **8**, e55126
34. Soysa, H. S. M., Aunkham, A., Schulte, A., and Suginta, W. (2020) Single-channel properties, sugar specificity, and role of chitoporin in adaptive survival of *Vibrio cholerae* type strain O1. *J. Biol. Chem.* **295**, 9421–9432
35. Soysa, H. S. M., Schulte, A., and Suginta, W. (2017) Functional analysis of an unusual porin-like channel that imports chitin for alternative carbon metabolism in *Escherichia coli*. *J. Biol. Chem.* **292**, 19328–19337
36. Soysa, H. S. M., Suginta, W., Moonsap, W., and Smith, M. F. (2018) Chitosugar translocation by an unexpressed monomeric protein channel. *Phys. Rev. E* **97**, 052417
37. Aunkham, A., Zahn, M., Kesireddy, A., Pothula, K. R., Schulte, A., Baslé, A., *et al.* (2018) Structural basis for chitin acquisition by marine *Vibrio* species. *Nat. Commun.* **9**, 220
38. Aunkham, A., and Suginta, W. (2021) Probing the physiological roles of the extracellular loops of chitoporin from *Vibrio campbellii*. *Biophys. J.* **120**, 2124–2137
39. Suginta, W., Chumjan, W., Mahendran, K. R., Schulte, A., and Winterhalter, M. (2013) Chitoporin from *Vibrio harveyi*, a channel with exceptional sugar specificity. *J. Biol. Chem.* **288**, 11038–11046
40. Toratani, T., Suzuki, K., Shimizu, M., Sugimoto, H., and Watanabe, T. (2012) Regulation of chitinase production by the 5′-untranslated region of the *ybfM* in *Serratia marcescens* 2170. *Biosci. Biotechnol. Biochem.* **76**, 1920–1924
41. Suzuki, K., Suzuki, M., Taiyoji, M., Nikaidou, N., and Watanabe, T. (1998) Chitin binding protein (CBP21) in the culture supernatant of *Serratia marcescens* 2170. *Biosci. Biotechnol. Biochem.* **62**, 128–135
42. Biswas, S., Mohammad, M. M., Patel, D. R., Movileanu, L., and van den Berg, B. (2007) Structural insight into OprD substrate specificity. *Nat. Struct. Mol. Biol.* **14**, 1108–1109
43. Eren, E., Parkin, J., Adelanwa, A., Cheneke, B., Movileanu, L., Khalid, S., *et al.* (2013) Toward understanding the outer membrane uptake of small molecules by *Pseudomonas aeruginosa*. *J. Biol. Chem.* **288**, 12042–12053
44. Yildiz, O., Vinothkumar, K. V., Goswami, P., and Kühlbrandt, W. (2006) Structure of the monomeric outer-membrane porin OmpG in the open and closed conformation. *EMBO J.* **25**, 3702–3713
45. Suginta, W., Sanram, S., Aunkham, A., Winterhalter, M., and Schulte, A. (2021) The C2 entity of chitosugars is crucial in molecular selectivity of the *Vibrio campbellii* chitoporin. *J. Biol. Chem.* **297**, 101350
46. Toratani, T., Shoji, T., Ikehara, T., Suzuki, K., and Watanabe, T. (2008) The importance of chitobiase and *N*-acetylglucosamine (GlcNAc) uptake in *N,N′*-diacetylchitobiose [$(GlcNAc)_2$] utilization by *Serratia marcescens* 2170. *Microbiology (Reading)* **154**, 1326–1332
47. Katoh, K., Rozewicki, J., and Yamada, K. D. (2019) MAFFT online service: multiple sequence alignment, interactive sequence choice and visualization. *Brief. Bioinform* **20**, 1160–1166
48. Tayyab, S., Qamar, S., and Islam, M. (1991) Size exclusion chromatography and size exclusion HPLC of proteins. *Biochem. Educ.* **19**, 149–152
49. Montal, M., and Mueller, P. (1972) Formation of bimolecular membranes from lipid monolayers and a study of their electrical properties. *Proc. Natl. Acad. Sci. U. S. A.* **69**, 3561–3566
50. Luckey, M., and Nikaido, H. (1980) Specificity of diffusion channels produced by λ phage receptor protein of *Escherichia coli*. *Proc. Natl. Acad. Sci. U. S. A.* **77**, 167–171
51. Szewzyk, Z., Szewzyk, R., and Stenström, T. A. (1993) Growth and survival of *Serratia marcescens* under aerobic and anaerobic conditions in the presence of materials from blood bags. *J. Clin. Microbiol.* **31**, 1826–1830